Asymmetric crossing of the attractive and repulsive magnetic potential by Abrikosov vortices

V. K. Vlasko-Vlasov,[1] A. Glatz,[1,2] D. Rosenmann,[3] R. Divan,[3] and W.-K. Kwok[1]
[1]*Materials Sciences Division, Argonne National Laboratory, Argonne, Illinois 60439, USA*
[2]*Physics Department, Northern Illinois University, DeKalb, Illinois 60115, USA*
[3]*Center for Nanomaterials, Argonne National Laboratory, Argonne, Illinois 60439, USA*

(Received 20 August 2020; revised 11 October 2020; accepted 13 November 2020; published 30 November 2020)

We present studies of Abrikosov vortex motion across the magnetically charged edges of long thin ferromagnetic stripes placed above or under a thin superconducting film. The magnetic charges at the stripe edges form attractive or repulsive potential wells for vortices. Using a relatively small in-plane magnetic field to polarize the stripe edges and normal-to-plane magnetic field to induce up or down polarized vortices, we tune the attractive or repulsive stripe-vortex interactions. Imaging of the vortex dynamics reveals that the repulsive magnetic potential U_m^+ acts as a robust vortex pinning barrier, while the attractive U_m^- has practically no effect on the vortex motion irrespective of the position of the stripes located above or underneath the superconducting film. We analyze the observed asymmetry using equations of the overdamped vortex motion. The formal analytical solution yields an asymmetry, but the numerical modeling with and without noise terms does not confirm it. Instead, we find that the asymmetry is caused by the creation of spontaneous vortices at the maxima of U_m, which depends on the edge polarity and suppress U_m^-. Furthermore, our experiment and time-dependent Ginzburg-Landau simulations demonstrate that magnetic pinning dominates over vortex pinning due to corrugations of the superconducting layer deposited on top of the ferromagnetic stripes.

DOI: 10.1103/PhysRevB.102.174511

I. INTRODUCTION

The dynamics of Abrikosov vortices, each carrying a single magnetic flux quantum in superconductors controls the electromagnetic response of these materials and can define their multiple applications from high power machines and devices [1–5] to the prospective cryogenic microelectronics for information technologies [6–9]. The single flux quantum of individual vortices, $\Phi_0 = h/2e$, which is a universal physical constant defined by the electron charge e and the Planck constant h, can be used as a bit carrier in digital operations or as a switch in Josephson circuits (see Refs. [10,11], and references therein). Different approaches and architectures have been proposed to store and manipulate vortices for these purposes (see Refs. [12–15], and references therein). However, there are still no reliable techniques for manipulating single vortices en masse. One of the widely discussed routes is to use ferromagnetic/superconducting (FM/SC) hybrid structures, where magnetic elements can induce tunable local magnetic fields allowing the generation, pinning or propagation of vortices [16,17]. A large number of experiments confirmed that thin magnetic islands of different shapes and periodicity placed on top or underneath a superconducting film can efficiently alter the vortex dynamics, resulting in matching effects and directional vortex motion [18–21]. These matching effects in FM/SC hybrids with periodic magnetic structures and in pure SC films with regular shape variations (thickness modulations, lattices of holes, periodic corrugations), appear as sharp minima in the resistivity curves $R(H)$ or as cusps in magnetization $M(H)$ at fields corresponding to integer or half integer flux quanta, Φ_0, per unit cell. They are frequently observed close to the SC transition temperature, T_c, and associated with different physical phenomena, such as oscillations of T_c in the periodic structure due to flux quantization per unit cell, field-induced superconductivity due to the local compensation of stray fields around magnetic patterns by applied fields, and commensurate pinning of vortices by periodic patterns. In the majority of experiments, the magnetic elements were placed underneath the SC film. In this case, though the magnetic component of pinning was considered to be dominant, there could be a non-negligible effect arising from the corrugation of the SC film around the magnetic elements. In some cases, the periodic roughness of the SC film deposited on top of the magnetic pattern was considered to be the major pinning source [19].

At temperatures well below T_c, the matching features are often supplanted by enhanced vortex pinning from inherent materials defects and cannot be detected via transport measurements. In this case, the magnetic pattern/vortex interactions can be revealed by local probe microscopy (e.g., magnetic-force microscopy (MFM) [22] or scanning Hall probe [23]), but usually only under static conditions following field cooling. Thus the relative strength of the magnetic pinning and pinning by the SC film corrugations, especially at lower temperatures and under dynamic conditions, still remains an open question.

In our recent works [24–27] we studied the effect of thin magnetic stripes deposited on top of the superconducting film.

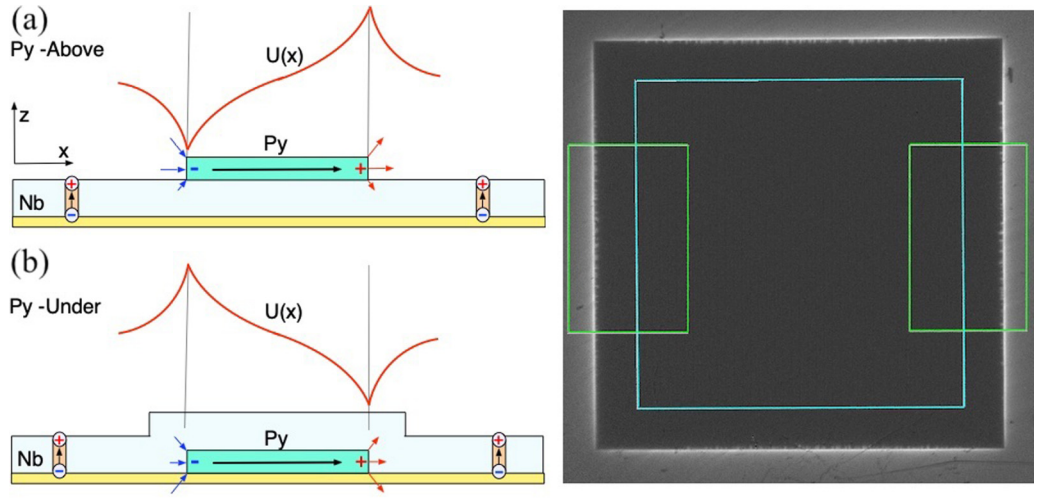

FIG. 1. Sketch of the magnetic fields and charges due to vortices polarized along z and magnetic stripes with $\mathbf{M}||x$. Long Py stripes are parallel to y (not shown) and are placed above (a) or underneath (b) the Nb film. $U(x)$ is the magnetic potential for vortices induced by the stripes. The right panel shows the MO image of the enhanced field at the sample edges in a small applied field H_z at $T < T_c$. The sample size is 2 × 2 mm. The blue square in the center outlines the area occupied by stripes, and green rectangles show areas of the MO images in Fig. 2.

We demonstrated that over a wide temperature range, the stripe edges act as magnetically charged lines, which strongly interact with the point-like magnetic charges of individual vortices. An appropriate picture of the magnetic monopole with $2\Phi_0$ charge, approximating their field above the superconductor, was presented by Carneiro and Brandt [28]. The interaction of the magnetic stripe edge and vortices depends on their mutual position and polarity. The perpendicularly polarized magnetic edge with a linear charge density $\rho_m = \mathrm{M}d_f$ (M is the magnetization and d_f is the the thickness of the FM film) repulses vortices of the same charge sign and attracts vortices of the opposite polarity. It mimics the interaction between an electrically charged line and a single electric charge decaying as $U_m \sim \mathrm{Log}(r)$ with the distance r between them. In the case of a thick SC film (thickness $d \gg \lambda$- SC penetration depth), when the stray field of the magnetic stripe edge is entirely screened by the Meissner current, its line charge doubles [29]. For a very thin SC film ($d \ll \lambda$), the account of the Meissner screening results in integral cosine and sine functions for the magnetic edge potential, which has a smaller amplitude but is qualitatively similar to the logarithmic U_m [25,26]. In this case, one would expect that when the vortex moves across oppositely charged stripe edges, the maximum strength, $(dU_m/dr)_{\max}$, of the repulsive and attractive barriers is equivalent and should require the same external force to cross either of them.

In our earlier experiments [25,26] we used long thin permalloy (Py) stripes *on top* of the niobium (Nb) film and varied the polarity of their edge charges by changing the direction of the in-plane field. Concurrently, by applying magnetic fields normal to the SC layer we could introduce vortices of a certain polarity and move them across the stripes. Unexpectedly, we found that the repulsive potential ($U_m{}^+$) from the stripe edges strongly delays the motion of positive vortices, while the attractive potential ($U_m{}^-$) has practically no effect. The strange asymmetry was explained by different kinetics of the vortex motion across $U_m{}^+$ and $U_m{}^-$.

In the present work, we compare the effect on the vortex motion for magnetic stripes placed *above* and *underneath* the superconducting layer and ascertain that the magnetic interactions between the stripe edges and vortices dominate over the effect of the SC film corrugations. In both cases the repulsive potential $U_m{}^+$ strongly impedes the vortex dynamics, while the attractive potential $U_m{}^-$ does not hinder the motion of vortices. We analyze this behavior using the viscous vortex motion equation with relevant coefficients retrieved from the experiment and propose that the difference in crossing $U_m{}^+$ and $U_m{}^-$ is due to the generation of extra vortices by the polarized magnetic stripe edges. In addition, we use the dynamic Ginzburg-Landau equations to model the vortex motion across the steplike bending of the superconducting film and confirm that the pinning energy by corrugations is noticeably smaller than the magnetic potential U_m.

II. EXPERIMENT

Periodic arrays of long 75-nm-thick Py stripes (80% Ni, 20% Fe), 30–35 μm wide, with 10–5 μm separation gap were fabricated using e-beam lithography and deposited either on top or under 100-nm-thick $\sim 2 \times 2$ mm superconducting ($T_c = 8.6$ K) Nb films (Fig. 1). The Nb films were grown on oxidized silicon wafers and were insulated from the Py patterns by chemical-vapor-deposited 10-nm SiO_2 layer to mitigate proximity effects. Both Py and Nb films were sputtered in a high vacuum magnetron system. The Py stripe patterns were positioned in the central area of the Nb squares leaving a $\sim$ 200-μm wide band of Nb at the perimeter.

The samples were placed on the cold finger of an optical cryostat and the distribution of the normal magnetic field on their surface was imaged with magneto-optics (MO) using garnet films with a large Verdet constant [30]. The Py stripes have in-plane magnetization, $\boldsymbol{M}$, which can be easily polarized in a desired direction with in-plane magnetic fields $\lesssim 50$ Oe. When $\boldsymbol{M}$ is aligned parallel to the length of the stripes, the

stray fields at their long edges are absent and show no MO contrast. Upon rotating $\boldsymbol{M}$ from the longitudinal direction, magnetic charges emerge at the stripe edges proportional to the component of $\boldsymbol{M}$ perpendicular to the edge face (with charge density $\rho_m = 4\pi \mathrm{div}\boldsymbol{M}$). The visual MO contrast of dark or bright color demonstrates the polarity and strength of the stray fields, H_s, at the stripe edges.

When a magnetic field, H_z, is applied normal to the sample surface, the Py magnetization (M_z) tilts only slightly out-of-plane due to the large shape anisotropy of the Py stripes. The same shape anisotropy defines the demagnetizing field ($H_d \sim -4\pi M_z$) which cancels the contribution of Py magnetization ($4\pi M_z$) to the normal magnetic flux. Thus, the change of the MO contrast in the applied normal field, at least in the field range used in our experiment, reveals only the distribution of superconducting vortices generated at $T < T_c$ allowing us to study their interactions with the Py stripe edges. Subtracting the images of the stray fields around the Py stripe edges taken before application of H_z, from the MO images obtained in $H_z \neq 0$ at $T < T_c$, yields a clear picture of the density of penetrating vortices and reveals their dynamics affected by the Py-edge potential.

III. RESULTS AND DISCUSSION

The main objective of this study is to compare the interaction of vortices with the attractive and repulsive potentials along the longitudinal Py stripe edges when the stripes are deposited *above* a *flat* Nb film and *under* the Nb film. In the latter case the Nb film is *corrugated* around the stripes as depicted in Fig. 1(b).

To set up the strongest magnetic coupling between the Py stripe edges and vortices, we cool the samples below T_c with an applied in-plane magnetic field perpendicular to the stripe length. Then a steadily increasing normal field H_z is applied to generate and move vortices from the sample boundaries towards and across the Py stripe edges.

Figure 2(a) shows the stray fields H_s after cooling the sample with Py stripes *above* the Nb film in an applied in-plane field directed as shown by the horizontal arrow. The resulting up and down H_s components in the zero applied normal field ($H_z = 0$) are revealed as bright and dark contrast. The corresponding sketch is shown in Fig. 1(a).

In the following MO images [Figs. 2(b)–2(f)] the initial H_s frame ($H_z = 0$) is subtracted from subsequent images, showing the spatial distribution of only the normal-to-surface flux in the sample at different H_z. When a large enough H_z is applied at $T < T_c$, vortices (bright contrast, positive B_z) first enter the Nb film from the edges and approach the region with the Py stripes [Fig. 2(b)]. With increasing H_z, the vortices are delayed and accumulated on the positively charged stripe edges. This is delineated in Fig. 2(c) by the increased contrast at the first stripe edge marked by the red arrow in the right-hand image and by the second stripe edge behind the blue arrow in the left-hand image. With further increasing H_z, the vortices cross the positive stripe edge while leaving a slightly reduced vortex density outside the stripe, and move further inwards until they are again hindered and accumulate at the next positively charged stripe edge [Figs. 2(d) and 2(e)]. The enhanced vortex density on one side of the positive stripe edge and the reduced vortex density on the other side indicate the enhanced pinning or the locally increased current along this edge. In contrast, the negatively charged stripe edges do not hinder vortex motion as delineated by the blue double-arrow in the left-hand images of Figs. 2(c)–2(e). A similar effect is observed after application of a strong normal field, raising the vortex density in the entire sample, followed by a reduction of H_z. Decreasing H_z pushes the vortices from the center towards the sample boundaries. As shown in Fig. 2(f), the same positively charged stripe edges impede flux exit. At the same time, the negatively charged edges do not show any effect on the exit of the positively charged vortices, although they impede the negatively charged vortices entering from the sample boundaries at $H_z \sim 0$. When the Py stripes are remagnetized with an opposite in-plane field, the stripe edge charges switch polarity and the newly formed lines of positive

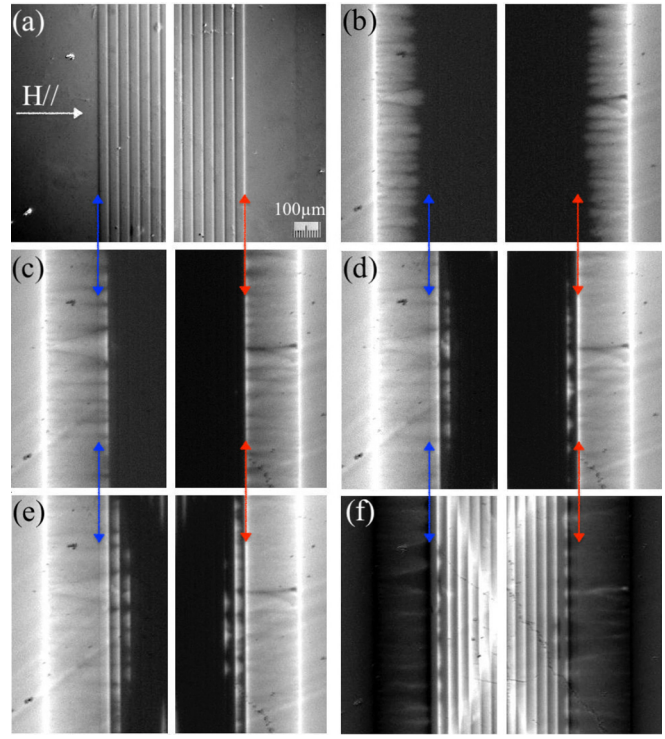

FIG. 2. MO images of the normal field distribution in areas outlined by green rectangles in Fig. 1 for Py stripes placed on top of the Nb film. (a) Stray fields of the stripes polarized along the horizontal arrow at $T > T_c$. Positively and negatively charged stripe edges are revealed by bright and dark contrast respectively. (b)–(e) normal flux entry with increasing applied field [$T = 4$ K, $H_z = 9.9$, 14.6, 17. 6, 21 Oe in (b) to (e)]. (f) trapped flux at $H_z = 0$ after application of 800 Oe. Double arrows show the position of the left and right sides of the stripe pattern. The dark negative (attractive) left edge does not hinder vortex motion. In contrast, vortices are delayed and accumulate at the bright (repulsive) positively charged edge on the right. When reducing H_z to zero, negative vortices, induced by the reversed critical currents, start to enter from the Nb square boundaries and are impeded at the negative stripe edge [dark contrast along left arrow in (f)] while they pass the positive stripe edge [right arrow in (f)]. Narrowing of the flux penetration front towards the sample center, well observed in Fig. 2(e), is due to the finite size of the sample where currents flow along the sides of the square.

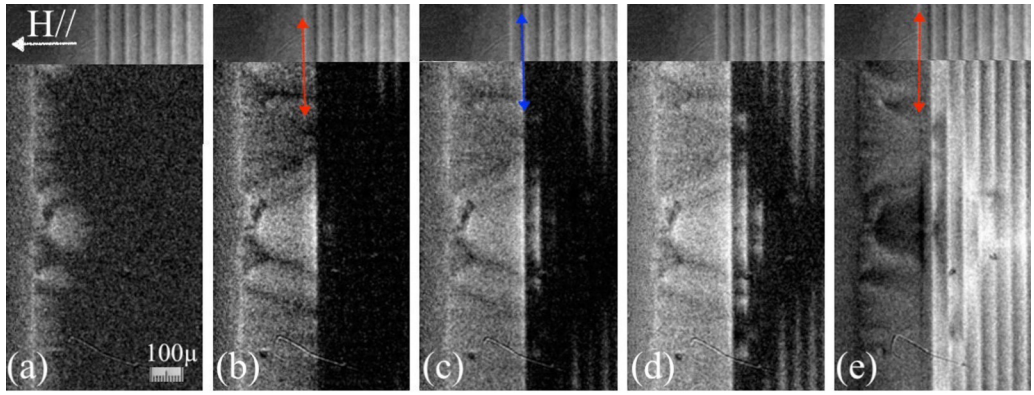

FIG. 3. Same as Fig. 2 but the Py stripes are under the Nb film. The position of stripes is presented in the top part of each panel. Positively and negatively charged stripe edges are bright and dark, respectively. $T = 4$ K, $H_z = 4.6$, 11.1, 15.4, 17.6 Oe in (a) to (d). (e) Positive flux (bright contrast) exit and negative flux (dark contrast) entry with reducing field from 800 to 8 Oe. Red double arrows show the left edge of the first Py stripe in (b) and (e), and the blue double-arrow in (c) shows the right edge of the first stripe. Unlike in Fig. 2, the negatively charged Py stripe edges impede vortices and the positive stripe edges does not affect their motion [in accordance with the sketch in Fig. 1(b)]. A slight contrast is observed along the positive Py stripe edge marked by red arrow in (b), which could be due to the Nb film corrugation. However, it is much weaker than the contrast on the negative stripe edge. In (e), the entry of negative vortices is inhibited (dark line along the double arrow) by the positively charged stripe edge.

magnetic charge hinder the motion of positive vortices while negatively charged Py-edges do not affect the vortex dynamics (not shown).

The same type of behavior is found in the samples with Py stripes placed underneath the Nb film as illustrated in Fig. 3. Although in this case, the negatively charged Py stripe edges delay the entry of positive vortices, while the positive stripe edges do not affect their motion as qualitatively explained by the sketch in Fig. 1(b). Our observations confirm that the asymmetry in the vortex motion across the repulsive and attractive potentials is essentially of magnetic nature, while the corrugation of the Nb film plays only a minor role.

For the case of magnetic stripes polarized along their length, the magnetic charges emerge only at their short ends. In this case, the stripes placed on top of the flat Nb film do not show any effect on the vortex motion across their long sides. When longitudinally polarized stripes are placed underneath the Nb film, their uncharged long sides show some effect but it is much weaker than that of the magnetically charged edges.

To understand the peculiarities of the magnetic vortex pinning by the Py stripes, we analyze the interactions between the stray fields at the magnetic stripe edges and the vortex flux. The interactions can be represented as a coupling of the vortex field outside of the SC film to the magnetization of the stripe (see, e.g., Ref. [31]). The easiest way to estimate the vortex-Py-edge coupling is to consider the magnetic charges at the stripe edge face repelling or attracting the effective magnetic charge of the vortex. The magnetic charge per unit length of the dz-wide line aligned with the Py-edge face is $\boldsymbol{M}dz$ (see Fig. 4), where $\boldsymbol{M}$ is the magnetization per unit volume of Py, and the field of this line charge at the position of the vortex is $H_l = Mdz/2\pi(z^2 + R^2)^{1/2}$.

The force on the pointlike vortex charge ($+$ or $-2\Phi_0$ [28]) from this line charge will be $dF_m = \Phi_0 MRdz/\pi(z^2 + R^2)$, such that the total force from the d_f-wide edge of the stripe placed at h_0 above the SC film, is

$$F_m = \pm(\Phi_0 MR/\pi)\int dz/(z^2 + R^2)|_{h0}{}^{h0+d_f}$$
$$= \pm(\Phi_0 M/\pi)\{\text{arctg}[(d_f + h_0)/R] - \text{arctg}(h_0/R)\}. \quad (1)$$

Then the Py-edge-vortex potential will be

$$U_m = \int dRF_m|_R{}^{R+D} = \mp(\Phi_0 M/\pi)[U(R + D) - U(R)] \quad (2)$$

with

$$U(R) = R\{\text{arctg}[(d_f + h_0)/R] - \text{arctg}(h_0/R)\}$$
$$+ (1/2)\{(d_f + h_0)\log[(d_f + h_0)^2 + R^2]$$
$$- h_0\log(h_0{}^2 + R^2)\}. \quad (3)$$

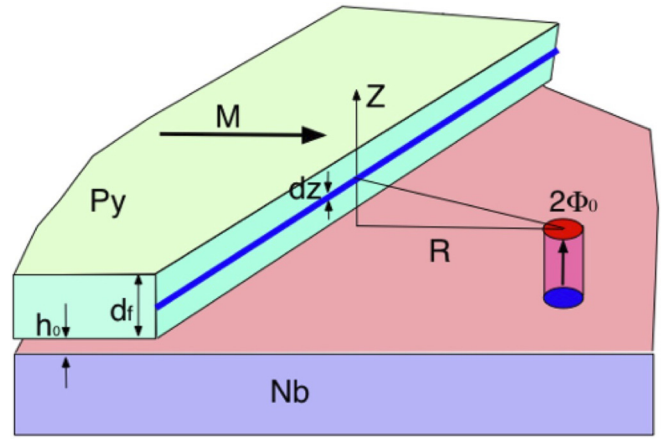

FIG. 4. Sketch of the geometry for estimating the stripe edge/vortex potential.

In Eq. (2) we accounted for the oppositely charged second edge of the magnetic stripe of width D to avoid the divergence of the integral.

Taking $d_f = 75\,\text{nm}$ and $h_0 = 10$ nm (values that correspond to our samples), and $\lambda = 84$ nm [32], we obtain a good fit for Eq. (1) with

$$F_{mf} = \pm(\Phi_0 M/\pi)ax/(x^2 + b^2), \tag{4}$$

where $a = 0.82$, $b = 0.42$, and $x = R/\lambda$. Now F_{mf} represents the force of a thin line with slightly reduced total magnetic charge at a height of 0.42λ above the SC film, located close to the middle of the Py-stripe edge (blue line in Fig. 4). The resulting potential U_{mf} decays as $-\log(x^2 + b^2)$, or as $-\log-\log x$ at $x \gg b$. Eq. (4) gives a convenient form for analyzing the overdamped motion of vortices across the edge barrier, which can be described by the Langevin equation:

$$-\eta dx/dt + F_{\text{mf}} + J\Phi_0 d_{\text{SC}} + \zeta(t) = 0. \tag{5}$$

Here $\eta = \eta_0 d_{\text{SC}}\lambda$ with η_0 being the Bardeen-Stephen viscosity, the third term is the Lorentz force of the SC current J in a d_{SC}-thick SC film, and $\zeta(t)$ depicts the noise. We anticipate that $J = J_c$, the critical current associated with the inherent defect pinning of the SC film. The structure of $\zeta(t)$ is described below.

First, we discuss the solution of Eq. (5) without the noise term. In its dimensionless form, Eq. (5) reads

$$dx/d\tau + 2Kx/(x^2 + b^2) + 1 = 0, \tag{6}$$

where $\tau = t/t_0, t_0 = \eta_0\lambda/J_c\Phi_0$, and $K = \pm Ma/2\pi J_c d_{\text{SC}}$. The formal solution of this equation is

$$x + [K/(K^2 - b^2)^{1/2}][x_1\text{Log}(x - x_1) - x_2\text{Log}(x - x_2)] = \tau + \text{const} \tag{7}$$

with $x_{1,2} = K \pm [K^2 - b^2]^{1/2}$.

Using $M = 800\,\text{G}$ for Py, $J_c \sim 10^{11}\text{A}/m^2$ and $d_{\text{SC}} =$ 100nm for our Nb film, we obtain $|K| \sim 0.84$. An appropriate plot of the real part of Eq. (7) for $\pm K$ is shown in Fig. 5. Here, the retracting branches of the curves are unphysical and one would expect that the transition to the upper part of the vortex trajectory occurs as shown by arrows. The vortex crossing of the repulsive potential ($K > 0$) should be essentially delayed compared to the crossing of the attractive potential ($K < 0$).

However, the numerical modeling of Eq. (6) with chosen initial conditions yields a different picture of $x(t)$, as shown in Fig. 6. Here, the motion steadily slows to the rest position in the case of repulsive $U_m{}^+$, or initially accelerates and then stops in the case of attractive $U_m{}^-$. In the stop point, x_0, the force $F_d \sim J_c \sim 1/|K|$ is equal to the oppositely directed force of the potential.

When the driving force F_d exceeds the critical value (maximum force of the potential defined by $|K_c| = b$), i.e., at $|K| < b$, vortices start moving continuously across both barriers (Fig. 6), showing slowed and accelerated segments reminiscent of the lower branches presented in the formal solution (Fig. 5) and then smoothly transferring to the higher branches.

Accounting for noise $\zeta_n(t)$ in Eq. (6) allows crossing the barrier at smaller driving forces (Fig. 7), i.e., at $|K| > |K_c|$. We considered two choices of $\zeta_n(t)$: random number in the range

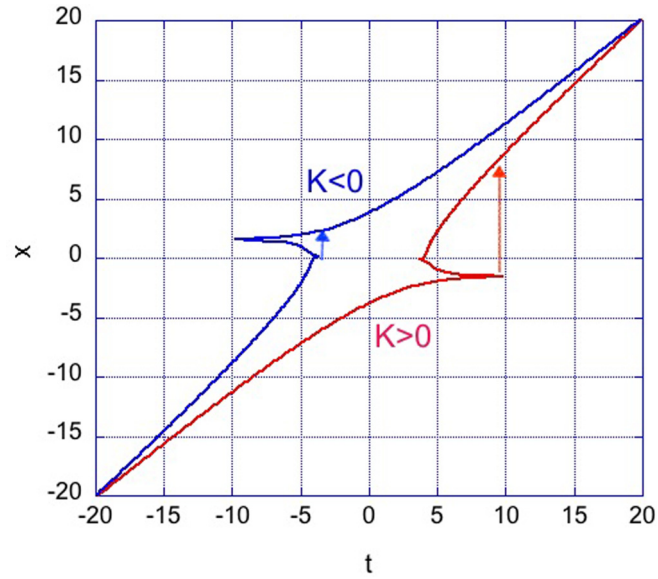

FIG. 5. Real part of the solution of Eq. (7), for the attractive $K = -0.84$ (blue) and repulsive $K = +0.84$ (red) potential with b = 0.42. Retracting branches are unphysical and the system should transfer from lower to higher branches via jumps, as shown by arrows.

$\pm\,\zeta_{\text{max}}$ (bipolar noise) and between 0 and $+\zeta_{\text{max}}$ (monopolar noise). The noise mimics the effect of temperature and accidental knocks from other vortices. The monopolar noise, suggests preferential knocks from new vortices coming from the sample boundaries. It is equivalent to an additional driving force and causes the crossing of the barrier at smaller ζ_{max} compared to the bipolar noise. However, for both bipolar and

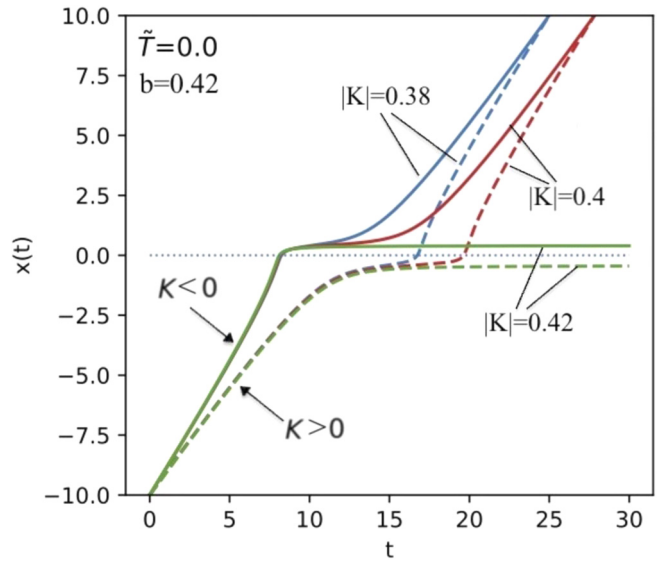

FIG. 6. Trajectories of vortices in the vicinity of the stripe edges obtained by numerical modeling of Eq. (6). Dimensionless $x(t)$ are shown for decreasing driving forces (increasing $|K|$) for attractive ($K < 0$) and repulsive ($K > 0$) potentials. At a critical driving force, $|K_c| = 0.42$, vortices halt in the stop points $+/-x_1$. At a larger force, $|K| < |K_c|$, they pass (although asymmetrically) both $K > 0$ and $K < 0$ barriers.

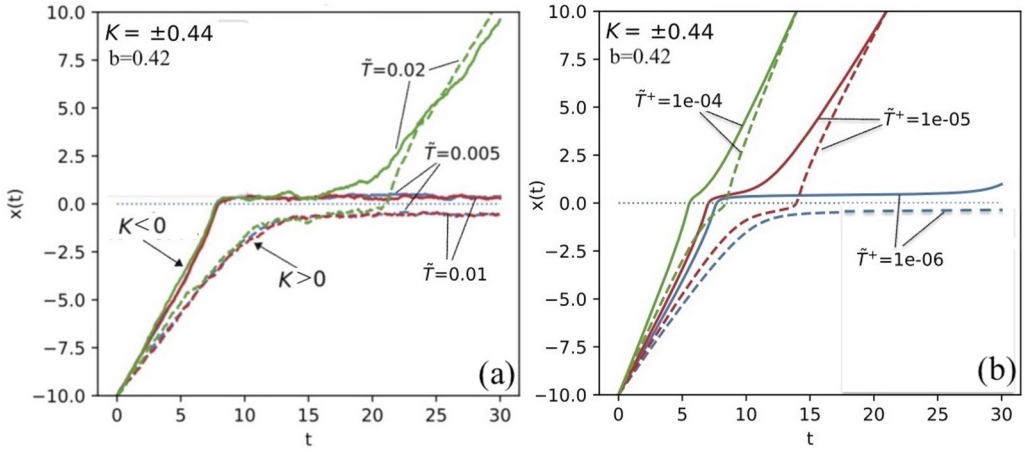

FIG. 7. Vortex trajectories with driving force below critical ($1/|K| < 1/|K_c|$) in the presence of bipolar (a) and monopolar (b) noise. The random noise amplitude is defined as $\zeta_{\max} = (3\tilde{T}/h_t)^{1/2}$ with an effective temperature $\tilde{T}$ and time step of the calculations h_t.

monopolar noise, it is hard to see a noticeable difference in the probability of crossing $U_m{}^-$ and $U_m{}^+$.

Therefore, numerical modeling shows that the viscous vortex motion alone cannot explain the observed difference in the vortex crossing of the attractive and repulsive magnetic barriers by considering only the effect of stray fields H_s at the magnetic stripe edges. An additional factor, which is not accounted for in Eq. (5), is the local creation of additional vortices along these edges induced by the same H_s. To estimate the probability of this process, it is necessary to compare the energy of the created vortex line in the SC film $E_v \sim d_{sc}\ (\Phi_0/4\pi\lambda)^2[\ln(\lambda/\xi) + 0.5]$ with the height of the magnetic potential, estimated from Eq. (4) as $U_m \sim (\Phi_0 M\lambda/2\pi)a\ln(x^2 + b^2 \sim \alpha(\Phi_0 M\lambda/2\pi)$ with $\alpha \sim 0.34$. The the creation of new vortices will occur at $M \gtrsim (\Phi_0/\alpha 8\pi\lambda^2)$ $[\ln(\lambda/\xi) + 0.5]d_{sc}/\lambda$. This condition is realized in our samples at all temperatures. When Py stripes are *above* the Nb film, negative vortices will be formed under the positively charged stripe edges and positive vortices under the negatively charged edges. The negative vortices induced under the positive edge will attract positive vortices entering the sample and reduce the height of the repulsive $U_m{}^+$. In turn, the positive induced vortices under the negative edge will repulse the new positive vortices and reduce the depth of the attractive $U_m{}^-$. However, when new positive vortices approach the Py-stripe edge, they annihilate the negative induced vortices and restore the height of $U_m{}^+$. At the same time, the new positive vortices under the negative attractive edge will only reduce the depth of $U_m{}^-$. As a result, the repulsive magnetic barrier $U_m{}^+$ is successively enhanced and the attractive barrier $U_m{}^-$ is suppressed due to the accumulation of entering vortices in their vicinity. We suggest this factor as the main reason for the observed asymmetry of the vortex motion across differently polarized magnetic edges.

In the case of the Py-stripes *under* the Nb film, U_m will be slightly altered, which can be described as a change of the effective distance of the magnetic stripe below the superconductor [parameter b in Eq. (4)]. Also, Meissner screening will be modified due to the corrugation of the SC layer near the stripe edges. The positively charged stripe edges now become attractive and the negatively charged edges become repulsive for the positive vortices [Fig. 1(b)]. In turn, the stray fields of the positive stripe edge induce positive vortices that suppress the attractive potential. At the same time, negative vortices induced at the negative stripe edge are annihilated by the entering positive vortices, thus restoring the repulsive potential. Although $U_m{}^+$ and $U_m{}^-$ switch sides on the stripes, depending on whether the Py stripes are underneath or atop the SC film (Fig. 1), the main physical picture of the stripe edge/vortex interaction remains the same, as we also see in the experiment.

An additional pinning should arise due to the increased length of the vortex crossing the corrugated section for Py-stripes placed underneath the Nb film. A rough estimate of the added extension of the vortex length is $\Delta l \sim [(2)^{1/2} - 1]d_{sc,}$, which will increase the vortex energy by $\Delta U_v \sim 0.4E_v$. This $\Delta U_v > 0$ will enhance the repulsive magnetic barrier, but will reduce the attractive U_m, similar to the effect of H_s-induced vortices. Yet, ΔU_v remains several times smaller than $|U_m|$ leaving the magnetic interactions dominant.

A more accurate analysis of ΔU_v follows from the computer simulations of the vortex motion against the corrugation of the SC film using the time-dependent Ginzburg-Landau model [33]. Movies of vortices crossing the corrugation under the constant current conditions are presented in the Supplemental Material [34,35]. By monitoring the time variations of the vortex energy, we obtain $\Delta U \sim 0.5E_v$ (a half of the vortex energy in the flat Nb film), which is in a reasonable agreement with our simple analytical estimate.

IV. CONCLUSIONS

Using direct magneto-optical imaging we studied the motion of Abrikosov vortices across the edges of thin in-plane magnetized permalloy stripes placed atop or underneath a niobium film to discern the effect of magnetic interaction and film corrugation on vortex pinning and dynamics. In-plane polarization of the Py stripes perpendicular to their length creates lines of positive or negative magnetic charges at the stripe edges resulting in lines of attractive $U_m{}^-$ or repulsive

U_m^+ potentials acting on magnetic monopoles corresponding to vortices in the SC layer. We mapped the spatial distribution of vortices in various U_m^- and U_m^+ depending on the Py stripe polarization and on the polarity of vortices created by opposite normal-to-plane fields.

Remarkably, for both cases with Py stripe arrays on top and underneath the Nb film, we found that the repulsive magnetic potential strongly hinders the vortex motion, while the attractive potential shows negligible effect on their dynamics.

We analyzed our observations using approximation of the one-dimensional overdamped vortex motion across a logarithmic magnetic potential of charged magnetic lines under the constant applied drive. The formal analytical solution of the viscous motion equation shows an asymmetry. However, the numerical treatment with and without the noise did not reveal a qualitative difference between U_m^+ and U_m^-. We then estimated the conditions for the vortex nucleation by the stray fields from the charged edges, which pointed to the existence of the spontaneous vortices of different polarities near the extrema of U_m. Near the maximum of the repulsive potential these vortices have the polarity opposite to that of new vortices induced by the applied normal field. Following the pattern of stray fields, they should be polarized downwards near the positive stripe edge in Fig. 1(a) and near the negative stripe edge in Fig. 1(b). As a result, these vortices should attract the upward polarized new vortices and thus reduce the strength of the repulsive potential. In turn, near the minimum of the attractive U_m, the spontaneous vortices are polarized parallel to the new vortices [upwards near the negative stripe edge in Fig. 1(a) and near the positive stripe edge in Fig. 1(b)]. So they will repulse the incoming vortices and thus reduce the strength of the attractive potential. However, when new vortices approach the extrema of U_m, they will annihilate with opposite spontaneous vortices formed at the repulsive edge and restore the strength of the repulsive U_m, which will then grow due to the accumulation of pinned vortices. At the same time, when approaching the attractive potential, the new vortices will only add there and further reduce the depth of the attractive U_m. This scenario explains the observed asymmetric action of oppositely charged stripe edges.

We conclude that the magnetic structures with in-plane magnetizations can be used as tunable potentials for efficient manipulation with Abrikosov vortices. Our MO observations, analysis of the vortex motion equations, and Ginzburg-Landau simulations reveal that vortex interactions with magnetic patterns are essentially stronger than the effects of pinning by film corrugations.

ACKNOWLEDGMENTS

This work was supported by the U.S. Department of Energy (DOE), Office of Science, Materials Sciences and Engineering Division. We used sample manufacturing facilities of the Center for Nanoscale Materials, supported by the U.S. DOE, Office of Science, Office of Basic Energy Sciences, under Contract No. DE-AC02-06CH11357.

[1] A. Gurevich, Challenges and opportunities for applications of unconventional superconductors, Ann. Rev. Condens. Matter Phys. **5**, 35 (2014).

[2] D. C. van der Laan, J. D. Weiss, and D. M. McRae, Status of CORC (R) cables and wires for use in high-field magnets and power systems a decade after their introduction, Supercond. Sci. Technol. **32**, 033001 (2019).

[3] P. Mukherjee and V. V. Rao, Design and development of high temperature superconducting magnetic energy storage for power applications - A review, Physica C **563**, 67 (2019).

[4] P. Bernstein and J. Noudem, Superconducting magnetic levitation: principle, materials, physics and models, Supercond. Sci. Technol. **33**, 033001 (2020).

[5] A. Bussmann-Holder and H. Keller, High-temperature superconductors: underlying physics and applications, Zeitschr. Naturforsch. B **75**, 3 (2020).

[6] G. Wendin, Quantum information processing with superconducting circuits: a review, Rep. Prog. Phys. **80**, 106001 (2017).

[7] R. Wordenweber, Engineering of superconductors and superconducting devices using artificial pinning sites, Phys. Sci. Rev. **2**, 20178000 (2017).

[8] A. I. Braginski, Superconductor electronics: Status and outlook, J. Supercond. Nov. Magn. **32**, 23 (2019).

[9] A. N. McCaughan, V. B. Verma, S. M. Buckley, J. P. Allmaras, A. G. Kozorezov, A. N. Tait, S. W. Nam, and J. M. Shainline, A superconducting thermal switch with ultrahigh impedance for interfacing superconductors to semiconductors, Nat. Electron. **2**, 451 (2019).

[10] T. Golod, A. Iovan, and V. M. Krasnov, Single Abrikosov vortices as quantized information bits, Nat. Comm. **6**, 8628 (2015).

[11] N. Satchell, Controlled superconducting vortex creation raises hope for a dissipationless memory device, Supercond. Sci. Technol. **32**, 020501 (2019).

[12] L. V. Belevtsov, Quasi-2D vortex memory cells? Mod. Phys. Lett. B **15**, 183 (2001).

[13] O. V. Dobrovolskiy, Abrikosov fluxonics in washboard nanolandscapes, Physica C **533**, 80 (2017).

[14] S. A. Haider, S. R. Naqvi, T. Akram, M. Kamran, and N. N. Qadri, Modeling electrical properties for various geometries of antidots on a superconducting film, Appl. Nanosci. **7**, 933 (2017).

[15] H. Polshyn, T. Naibert, and R. Budakian, Manipulating multivortex states in superconducting structures, Nano Lett. **19**, 5476 (2019).

[16] M. Velez, J. I. Martin, J. E. Villegas, A. Hoffmann, E. M. Gonzalez, J. L. Vicent, and I. K. Schuller, Superconducting vortex pinning with artificial magnetic nanostructures, J. Magn. Magn. Mater. **320**, 2547 (2008).

[17] A. Yu. Aladyshkin, A. V. Silhanek, W. Gillijns, and V. V. Moshchalkov, Nucleation of superconductivity and vortex matter in superconductor-ferromagnet hybrids, Supercond. Sci. Technol. **22**, 053001 (2009).

[18] V. Rouco, R. Cordoba, J. M. De Teresa, L. A. Rodriguez, C. Navau, N. Del-Valle, G. Via, A. Sanchez, C. Monton, F. Kronast, X. Obradors, T. Puig, and A. Palau, Competition between superconductor – ferromagnetic stray magnetic fields in

$YBa_2Cu_3O_{7-x}$ films pierced with Co nano-rods, Sci. Rep. **7**, 5663 (2017).

[19] J. del Valle, A. Gomez, J. Luis-Hita, V. Rollano, E. M. Gonzalez, and J. L. Vicent, Different approaches to generate matching effects using arrays in contact with superconducting films, Supercond. Sci. Technol. **30**, 025014 (2017).

[20] V. Rollano, A. Munoz-Noval, A. Gomez, F. Valdes-Bango, J. I. Martin, M. Velez, M. R. Osorio, D. Granados, E. M. Gonzalez, and J. L. Vicent, Topologically protected superconducting ratchet effect generated by spin-ice nanomagnets, Nanotechnol. **30**, 244003 (2019).

[21] O. V. Dobrovolskiy, E. Begun, V. M. Bevz, R. Sachser, and M. Huth, Upper Frequency Limits for Vortex Guiding and Ratchet Effects, Phys. Rev. Appl. **13**, 024012 (2020).

[22] T. Shapoval, V. Metlushko, M. Wolf, B. Holzapfel, V. Neu, and L. Schultz, Direct observation of superconducting vortex clusters pinned by a periodic array of magnetic dots in ferromagnetic/superconducting hybrid structures, Phys. Rev. B **81**, 092505 (2010).

[23] E. Marchiori, P. J. Curran, J.-Y. Kim, N. Satchell, G. Burnell, and S. J. Bending, Reconfigurable superconducting vortex pinning potential for magnetic disks in hybrid structures, Sci. Rep. **7**, 45182 (2017).

[24] V. K. Vlasko-Vlasov, F. Colauto, T. Benseman, D. Rosenmann, and W.-K. Kwok, Triode for magnetic flux quanta, Sci. Rep. **6**, 36847 (2016).

[25] V. K. Vlasko-Vlasov, F. Colauto, A. I. Buzdin, D. Rosenmann, T. Benseman, and W.-K. Kwok, Magnetic gates and guides for superconducting vortices, Phys. Rev. B **95**, 144504 (2017).

[26] V. K. Vlasko-Vlasov, F. Colauto, A. I. Buzdin, D. Rosenmann, T. Benseman, and W.-K. Kwok, Manipulating Abrikosov vortices with soft magnetic stripes, Phys. Rev. B **95**, 174514 (2017).

[27] V. K. Vlasko-Vlasov, F. Colauto, T. Benseman, D. Rosenmann, and W.-K. Kwok, Guiding thermomagnetic avalanches with soft magnetic stripes, Phys. Rev. B **96**, 214510 (2017).

[28] G. Carneiro and E. H. Brandt, Vortex lines in films: Fields and interactions, Phys. Rev. B **61**, 6370 (2000).

[29] E. B. Sonin, Suppression of superconductivity (weak link) by a domain wall in a two-layer superconductor-ferromagnet film, Sov. Tech. Phys. Lett. **14**, 714 (1988) [Pis'ma Zh. Tekh. Fiz. **14**, 1640 (1988)].

[30] V. K. Vlasko-Vlasov, G. W. Crabtree, U. Welp, and V. I. Nikitenko, Magneto-optical studies of magnetization processes in high-Tc superconductors, NATO ASI Ser. E **356**, 205 (1999).

[31] M. V. Milosevic and F. M. Peeters, Vortex pinning in a superconducting film due to in-plane magnetized ferromagnets of different shapes: The London approximation, Phys. Rev. B **69**, 104522 (2004).

[32] V. K. Vlasko-Vlasov, F. Colauto, A. A. Buzdin, D. Carmo, A. M. H. Andrade, A. A. M. Oliveira, W. A. Ortiz, D. Rosenmann, and W.-K. Kwok, Crossing fields in thin films of isotropic superconductors, Phys. Rev. B **94**, 184502 (2016).

[33] I. A. Sadovskyy, A. E. Koshelev, C. L. Phillips, D. A. Karpeyev, and A. Glatz, Stable large-scale solver for Ginzburg-Landau equations for superconductors, J. Comput. Phys. **294**, 639 (2015).

[34] See Supplemental Material at http://link.aps.org/supplemental/10.1103/PhysRevB.102.174511 for a movie of the vortex motion across the z-shape folding in the superconducting film. The parameters of the simulations are described in Ref. [35].

[35] See Supplemental Material at http://link.aps.org/supplemental/10.1103/PhysRevB.102.174511 for details about the geometry and parameters used in the simulations of Ref. [34], and pictures of flux entry at different stripe polarizations.